

A cluster-based mean-field, perturbative and coupled-cluster theory description of strongly correlated systems

Athanasios Papastathopoulos-Katsaros,^{1, a)} Carlos A. Jiménez-Hoyos,² Thomas M. Henderson,^{1,3} and Gustavo E. Scuseria^{1,3}

¹⁾*Department of Chemistry, Rice University, Houston, Texas 77005, USA*

²⁾*Department of Chemistry, Wesleyan University, Middletown, Connecticut 06459, USA*

³⁾*Department of Physics and Astronomy, Rice University, Houston, Texas 77005, USA*

(Dated: 19 February 2021)

We introduce cluster-based mean-field, perturbation and coupled-cluster theories to describe the ground state of strongly-correlated spin systems. In cluster mean-field, the ground state wavefunction is written as a simple tensor product of optimized cluster states. The cluster-language and the mean-field nature of the ansatz allows for a straightforward improvement based on perturbation theory and coupled-cluster, to account for inter-cluster correlations. We present benchmark calculations on the 2D square $J_1 - J_2$ Heisenberg model, using cluster mean-field, second-order perturbation theory and coupled-cluster. We also present an extrapolation scheme that allows us to compute thermodynamic limit energies very accurately. Our results indicate that, even with relatively small clusters, the correlated methods can provide an accurate description of the Heisenberg model in the regimes considered. Some ways to improve the results presented in this work are discussed.

I. INTRODUCTION

Spin lattices and more specifically, Heisenberg models, are of significant chemical importance. For example, iron-sulfur clusters relevant to nitrogen fixation or photosynthesis, such as ferredoxins, have been treated according to the Heisenberg model.¹ Single molecule magnets have possible applications in quantum computers as the smallest practical unit for magnetic memory. These molecules are usually metal clusters, and the magnetic coupling between the spins of the metal ions can also be described by a Heisenberg Hamiltonian.² Lastly, electrified, conjugated hydrocarbons and a few superconductors have some of their features modelled after Heisenberg exchange interactions.³⁻⁵ A common feature of all those systems is that they are strongly-correlated.

Despite tremendous effort and progress, the accurate and efficient description of the ground state of strongly-correlated systems represents an open problem in quantum chemistry. The defining feature of strongly-correlated systems is their multi-reference nature, which makes single-reference methods inadequate.⁶ Accordingly, approaches based on composite particles have been proposed for treating these systems, e.g. resonating valence bond as a ground state candidate for high- T_c superconductors, suggested by Anderson.⁷

In this work, which is a continuation of the work in Ref. 8, we use composite many-spin cluster states to describe the ground state of strongly-correlated spin lattices. More specifically, we divide the lattice into clusters, each containing a predefined number of sites which in this work are chosen using proximity in the lattice. These clusters can have any shape and any size, although for 2D systems, compact shapes provide better results. The cluster states are a subset of all the available many-particle states (most often all the states of the $S_z = 0$ sector). We presume that an accurate zero-th order description of the ground state of the full system can be prepared

as a product of cluster states. It is important to note that the many-particle state in each cluster is determined in the presence of other clusters. The resulting cluster mean-field (cMF) state is variational. The optimization provides not only the optimal cMF state, but also a renormalized Hamiltonian expressed in terms of cluster states. Traditional many-body approaches can then be used, on this renormalized Hamiltonian, to account for the missing inter-cluster correlations.

In related work, Isaev, Ortiz, and Dukelsky⁹ considered, in their hierarchical mean-field (HMF) approach, a similar ansatz to ours for the same Hamiltonian. Our approach differs from that used in Ref. 9 in not requiring the individual clusters to share the same ground state. That is, the ground state of each cluster is optimized independently allowing for (translational and spin) symmetry-broken solutions. In addition, we here consider two common approaches from quantum chemistry, Rayleigh-Schrödinger perturbation theory (RS-PT)¹⁰ to second-order and coupled-cluster (CC)¹¹ as a means to obtain a correlated approach defined in terms of clusters. Our coupled-cluster approach is inspired by Li's¹² block-correlated coupled-cluster method. In that work, however, the ground state of each cluster was not optimized in the presence of other clusters as we do here. Block-correlated coupled cluster has been used with high success in quantum chemistry to describe strongly-correlated molecular systems using a complete active-space^{13,14} reference state. In addition, Mayhall¹⁵ went beyond cMF by implementing a selective configuration interaction framework and had very accurate results for fermionic systems. Lastly, a cluster product state is also connected with tensor network (TN) techniques that have been gaining popularity for treating strongly-correlated systems.¹⁶ For more information on this connection and the advantages of cMF in contrast to other more sophisticated approaches, we refer the reader to Ref. 8.

There are many positive aspects that cMF possesses, which we would like to point out. First of all, straightforward symmetry breaking (S^2 symmetry) can partially account for inter-cluster correlations. Moreover, the fact that the cluster mean-

^{a)}Electronic mail: athanasios.papastathopoulos-katsaros@rice.edu

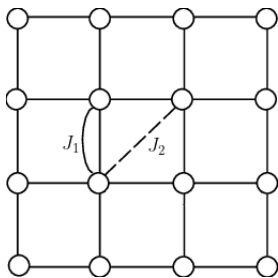


FIG. 1. Nearest-neighbor (J_1) and next-nearest neighbor (J_2) interactions.

field state constitutes the ground state of a mean-field Hamiltonian of which the full set of eigenstates can be easily constructed, allows us to exploit already developed techniques from the single-reference family of methods, in order to account for the missing inter-cluster correlations.

Our objective with this work is two-fold. First, we present the cMF formalism and provide details of the RS-PT (cPT2) and the coupled-cluster formulation we use (cCCSD). Our second objective is to apply these techniques to a simple strongly-correlated system: the Heisenberg model in a 2D square lattice. It is important to underline that the 1D case is exactly solvable,¹⁷ so we will focus our attention on the 2D model. This model has received numerous studies in the past two decades, using various methods such as exact diagonalization,^{18–23} coupled-cluster,^{24–26} density-matrix renormalization group (DMRG),²⁷ matrix-product or tensor-network based algorithms,^{28–30} resonating valence bond (RVB)³¹ and quantum Monte Carlo (QMC).³² We compare our results with calculations from Ref. 20, which we use as a reference. Those results are not exact in the thermodynamic limit, because they are extrapolated from different 2D shapes (more information in Ref. 20), but we consider them useful for a semi-quantitative comparison. Our results show that cPT2 and cCCSD significantly improve upon cMF and can provide an accurate description of the ground state of the square J1-J2 Heisenberg lattice.

The rest of the article is organized as follows. In Sec. II we present the formalism behind cMF, cPT2 and cCCSD. Section III provides some practical computational details regarding the calculations presented in this work. In Sec. IV we present the results of cMF, cPT2 and cCCSD calculations for the 2D square $J_1 - J_2$ Heisenberg model. A brief discussion following the results is presented in Sec. V, as well as some ideas as to how to improve the approaches presented here. Lastly, Sec. VI is dedicated to some general conclusions.

II. FORMALISM

A. Heisenberg model

In this work, we focus our attention on the $J_1 - J_2$ Heisenberg model in two-dimensions on a square grid. The Heisenberg model describes a collection of spins in a lattice (of finite

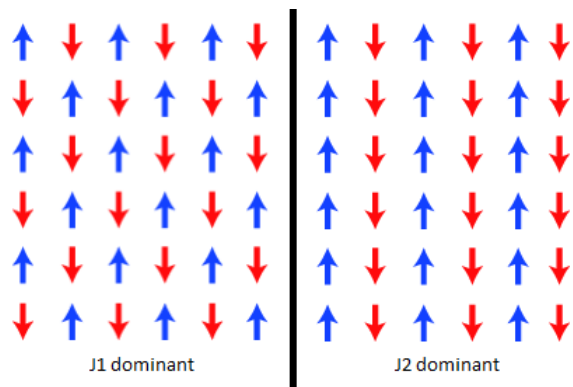


FIG. 2. Néel (left) and collinear (right) antiferromagnetic phases of the square $J_1 - J_2$ Heisenberg model. In between, there is a non-magnetic phase whose exact form is debated.

size L) interacting through the Hamiltonian

$$\hat{H} = J_1 \sum_{\langle ij \rangle} \vec{S}_i \cdot \vec{S}_j + J_2 \sum_{\langle\langle ij \rangle\rangle} \vec{S}_i \cdot \vec{S}_j \quad (1)$$

where \vec{S}_i is the spin- $\frac{1}{2}$ operator on site i , J_1 and J_2 are the nearest-neighbor and the next-nearest neighbor coupling coefficients respectively (see Fig. 1), and the notation $\langle ij \rangle$ implies interaction among nearest-neighbors, while $\langle\langle ij \rangle\rangle$ implies interaction among next-nearest neighbors. In the following, we confine ourselves to the antiferromagnetic (AFM) case $J_1, J_2 > 0$.

As mentioned previously, this model has been studied extensively in the past two decades, using various methods. It has been established that in the regime $0 \lesssim J_2/J_1 \lesssim 0.4$, the ground state is an antiferromagnetic (AFM) phase with Néel order, due to the dominance of the nearest-neighbor interactions J_1 . In $J_2/J_1 \gtrsim 0.6$, the ground state displays an AFM phase with collinear long-range order character due to the dominance of the next-nearest-neighbor coupling J_2 (see Fig. 2). In the regime $0.4 \lesssim J_2/J_1 \lesssim 0.6$, the Néel and the collinear orders compete. The nature of this intermediate ground state is still a much debated issue,^{9,19,27,30,33–38} as are the type of the phase transitions and the transition points. Because cMF has already been used to shed light on these topics (see Ref. 39) we will not focus our attention on these issues, but we need to mention there is a second-order transition from the Néel to the paramagnetic phase, whereas there is a first-order transition from the paramagnetic to the collinear antiferromagnetic phase.

B. Cluster Mean-Field

Our formalism of cluster mean-field (cMF) is based on Ref. 8, but in this paper we confine ourselves to the spin case, which consists of a subset of configurations found in fermionic systems. For more details we refer the reader to that work, but below we present the general framework.

Let the lattice states be grouped, according to some criterion (such as proximity in real space), into clusters of size

l_1, l_2, \dots, l_n , where n is the number of such clusters. Formally, the Hilbert space of each cluster is of size 2^{l_i} , as in each site we can either have a spin-up or a spin-down. We choose to work with eigenstates of S_z in each cluster, thereby reducing the effective dimension of the Hilbert space. Similarly to Ref. 27, the Hilbert space of the full system is simply given by the tensor product of the Hilbert spaces of all clusters.

A second-quantized formulation in terms of cluster product states can also be established. Let $A_{I,c}^\dagger$ ($A_{I,c}$) create (annihilate) the I -th state in cluster c . This I -th state is a linear combination of many-spin basis states (possibly mixing states with different S_z) constructed as products of the states in the cluster. We formally write

$$|I\rangle_c = A_{I,c}^\dagger |-\rangle_c \quad (2)$$

where $|I\rangle_c$ is the vacuum state in cluster c , a useful abstract construct.

Each cluster product state is formally built as

$$|I\rangle_1 |J\rangle_2 \dots |Z\rangle_n \equiv A_{I,1}^\dagger A_{J,2}^\dagger \dots A_{Z,n}^\dagger |-\rangle \quad (3)$$

where $|-\rangle$ is a vacuum state for the full system. In this work, we consider a cluster product (mean-field) state as a variational ansatz for the ground state wavefunction. That is, the ansatz $|\Phi_0\rangle$ for the ground state is given by

$$|\Phi_0\rangle = |0\rangle_1 |0\rangle_2 \dots |0\rangle_n \quad (4)$$

where the 0 label indicates the ground state of each cluster in the presence of the other clusters. The lowest energy cMF state is obtained by a variational minimization scheme, as outlined in Ref. 8.

Defining excited configurations is straightforward. We can write them as

$$|\Phi_{Ii}\rangle = |0\rangle_1 \dots |I\rangle_i \dots |0\rangle_n, \quad (5)$$

$$|\Phi_{Ii;Jj}\rangle = |0\rangle_1 \dots |I\rangle_i \dots |J\rangle_j \dots |0\rangle_n, \quad (6)$$

$$|\Phi_{Ii;Jj;Kk}\rangle = |0\rangle_1 \dots |I\rangle_i \dots |J\rangle_j \dots |K\rangle_k \dots |0\rangle_n \quad (7)$$

for singly-, doubly-, and triply-excited clusters.

Before proceeding further, let us comment on the nature of the cluster product states considered in this work. We indicated above that the ground state of each cluster is expressed as a linear combination of the many-spin basis states in it. The expansion over those states can be restricted and for our purposes, we confine ourselves to cases with a specific S_z . This is done in order for the cluster product state $|\Phi_0\rangle$ to be an eigenfunction of S_z and to reduce the dimension of the ground state vector in each cluster. Lastly, we choose to break S^2 in each cluster to develop long-range antiferromagnetic ordering.

C. Matrix elements and cMF optimization

The evaluation of the matrix elements is again similar to Ref. 8, but an important difference that we need to point out is that the spin cluster Hamiltonian has 1- and 2-cluster elements but not 3- or 4-cluster elements. This difference arises

because of the form of the Hamiltonian, which does not have more than 2-spin interactions. This significantly simplifies the procedure for both the cMF optimization, as well as the cPT2 and cCC extensions mentioned later. For details regarding the cMF optimization, we refer the reader to Ref. 8. We note that the zero-th order cluster Hamiltonian for a given number of fermions is given by

$$\hat{H}_c^0 = \sum_{pr \in c} \langle p|\hat{t}|r\rangle a_p^\dagger a_r + \frac{1}{2} \sum_{pqrs} \langle pq|\hat{v}|rs\rangle a_p^\dagger a_q^\dagger a_s a_r + \sum_{pr \in c} a_p^\dagger a_r \sum_{c' \neq c} \sum_{qs \in c'} \rho_{sq}^{c'} (\langle pq|\hat{v}|rs\rangle - \langle pq|\hat{v}|sr\rangle) \quad (8)$$

where $\rho_{sq}^{c'}$ is the one-particle density matrix in cluster c' . We choose to perform the optimization self-consistently, in order to minimize the energy. The formula above was given in its fermionic form, since we expect most readers will be more familiar with fermionic Hamiltonians than spin Hamiltonians. Lastly, we remind the reader that this is a spin system so there is no orbital optimization to be considered.

We think one final comment contrasting cMF and standard diagonalization techniques is necessary. Let us focus on the case of a finite lattice with periodic boundary conditions. The scaling of cMF with respect to cluster size is similar to that of exact diagonalization performed on a full lattice of the same size as the cluster. cMF, however, has a larger prefactor since the equations need to be solved self-consistently and the ansatz explicitly breaks the translational (and, possibly, spin) symmetry of the lattice. Thus, we can reach cluster sizes comparable to those achievable with exact diagonalization results (though of course cMF can have many clusters). In this work, the largest cMF calculation reported used a 6x6 cluster, and the length of the eigenvector in each tile is $\sim 10^{10}$. Note also that we can use less costly approximate methods in each cluster instead to reduce the scaling of cMF. Also note that cMF allows us to find different solutions for different regimes.

D. Perturbation theory

Once again, the theory is very similar to Ref. 8, but significantly simplified. Generally, in RS-PT, the second-order correction to the ground state energy is evaluated as

$$E^{(2)} = \sum_{\mu \neq 0} \frac{|\hat{V}_{0\mu}|^2}{\epsilon_0 - \epsilon_\mu} \quad (9)$$

where $\hat{V} = \hat{H} - \hat{H}_0$ and $V_{0\mu} = \langle \Phi_0 | \hat{V} | \mu \rangle$. Here, μ labels the eigenstates of \hat{H}_0 and ϵ_μ are the corresponding eigenvalues. The excited states framework was explained in section B. As mentioned earlier, the evaluation of the matrix elements is easier compared to the fermionic case, because there are no 3- and 4-cluster interactions, so the cost of cPT2 is $\mathcal{O}(n^2 M^2)$, where M is the number of excited states in each cluster. We would like also to remind the reader that we use all the states in the Hilbert space of each cluster (although in practice for cPT2 we only need states with $S_z = m, m+1, m-1$, where m is the S_z value used in cMF), even though in the cMF optimization only one S_z sector of the Hilbert space was considered. In

addition, due to the structure of the Hamiltonian, we only have two types of 2-tile interactions (S_z -preserving and S_z mixing), as opposed to 5 (see Ref. 8) in the fermionic case.

E. Coupled-cluster theory

In this paper, our aim is to go beyond perturbation theory to a coupled-cluster framework. Our work bears connection to Ref. 12, but it is important to note that in that work, the ground state of each cluster was neither optimized in the presence of other clusters nor tested on the same model.

The cluster coupled-cluster (cCC) expansion of the ground-state wave function can be written in an intermediate normalized form as follows:

$$|\Psi\rangle = e^{\hat{T}} |\Phi_0\rangle \quad (10)$$

where \hat{T} is the cluster operator. In this work, we focus our attention to singles and doubles, therefore

$$\hat{T} = \hat{T}_1 + \hat{T}_2 \quad (11)$$

and in the cluster language, \hat{T}_1 and \hat{T}_2 operators can be written as

$$\hat{T}_1 = \sum_i \sum_{I(i)} t_i B_i^+ B_{0_i}^- \quad (12)$$

$$\hat{T}_2 = \frac{1}{2!} \sum_i \sum_{j \neq i} \sum_{I(i)} \sum_{J(j)} t_{i,j} B_i^+ B_{0_i}^- B_j^+ B_{0_j}^- \quad (13)$$

where the coefficients t_i and $t_{i,j}$ are the single and double amplitudes respectively, the operator B_i^+ excites cluster i to state I and operator $B_{0_i}^-$ de-excites cluster i to its ground state.

By projecting onto $|\Phi_0\rangle$ and the space of singly and doubly excited configuration functions, and by utilizing the fact that for spin systems we have up to 2-cluster excitations, the cCCSD equations naturally truncate and become

$$E_{cCCSD} = \langle \Phi_0 | H | \Phi_0 \rangle + \langle \Phi_0 | H | T_1 \Phi_0 \rangle + \langle \Phi_0 | H \left| \left(T_2 + \frac{1}{2} T_1^2 \right) \Phi_0 \right\rangle \quad (14a)$$

$$E_{cCCSD} t_i = \langle \Phi_i | H | \Phi_0 \rangle + \langle \Phi_i | H | T_1 \Phi_0 \rangle + \langle \Phi_i | H \left| \left(T_2 + \frac{1}{2} T_1^2 \right) \Phi_0 \right\rangle + \langle \Phi_i | H \left| \left(T_2 T_1 + \frac{1}{6} T_1^3 \right) \Phi_0 \right\rangle \quad (14b)$$

$$E_{cCCSD}(t_{i,j} + t_i t_j) = \langle \Phi_{i,j} | H | \Phi_0 \rangle + \langle \Phi_{i,j} | H | T_1 \Phi_0 \rangle + \langle \Phi_{i,j} | H \left| \left(T_2 + \frac{1}{2} T_1^2 \right) \Phi_0 \right\rangle + \langle \Phi_{i,j} | H \left| \left(T_2 T_1 + \frac{1}{6} T_1^3 \right) \Phi_0 \right\rangle + \langle \Phi_{i,j} | H \left| \left(\frac{1}{2} T_2^2 + \frac{1}{2} T_2 T_1^2 + \frac{1}{24} T_1^4 \right) \Phi_0 \right\rangle \quad (14c)$$

where eq. 14a is the equation for the energy, and 14b and 14c are for the single and double amplitudes respectively. If we insert eq. 12 and eq.13, we get a set of nonlinear equations and like in traditional coupled-cluster, we solve the equations self-consistently.

It should be emphasized that in a cCCSD calculation the computation of the last term in the right-hand side of eq.14c is the most time consuming step, which makes the cCCSD method computationally a $\mathcal{O}(n^4)$ procedure, where n is the number of clusters.

Lastly, similar to the conventional truncated CC expansion, the truncated cCC expansion is also size extensive. For more information on the proof, we encourage the reader to check Ref. 12.

III. COMPUTATIONAL DETAILS

The cMF, cPT2 and cCCSD calculations presented in this work were carried out with a locally prepared code. In all the calculations with even number of spins in each cluster, we use the same number of up and down spins, whereas in all the cases with odd number of spins, we use +/- number of up and down spins in order to be able to construct Néel and collinear antiferromagnetic phases respectively. In this work, we choose to work with eigenstates of S_z in each cluster for computational convenience. At this point, it is important to note that the S_z of each cluster is not a symmetry of the Hamiltonian, so this choice is a constraint on the cMF. The full relevant S_z sector of Hilbert space within each cluster was used in constructing the cluster ground state $|0\rangle_c$. For small cluster sizes, the ground state in each cluster was found by a standard diagonalization of the local cluster Hamiltonian. For larger cluster sizes, a Davidson⁴⁰ algorithm was used to solve for the ground state. In cPT2 and cCCSD calculations, we loop over all the relevant excited cluster states (although in principle the number of states can be truncated, which was done in Ref. 8). For solving the cCCSD equations, the traditional CC iteration scheme was used.⁴¹

IV. RESULTS

In this section we present results of cMF, cPT2 and cCCSD calculations on the 2D Heisenberg model. We start by providing the basic idea in Sec. IV A, where we dive into some details regarding the optimization of cMF states and the way

in which other results are presented. In Sec. IV B we show and compare the results from cPT2 to cMF calculations. In Sec. IV C, we show and compare our cCCSD results to the cMF and cPT2 ones. These results are compared to accurate numerical estimates from Ref. 20.

A. Basic idea

In this section we discuss most of the aspects regarding the optimization of cMF states. In this way, we hope that the results presented in subsequent sections will become more transparent to the reader. We consider rectangular Heisenberg periodic lattices with $J_1, J_2 \geq 0$. As a first step, we choose the corresponding tiling scheme (i.e., defining how the spins are grouped into clusters). The optimized state in the cluster is expressed as a linear combination of all the possible (combinatorial number) resulting configurations and it is optimized by a self-consistent diagonalization of the appropriate cluster Hamiltonian.

It is important to mention that we are interested in the thermodynamic limit properties (very large system sizes). This is achieved by having both the cluster size $l \rightarrow \infty$ and the system size $L \rightarrow \infty$. For this work, however, only a limited number of sizes was tried, because the exact diagonalization in large clusters becomes very expensive (recall that we require not only the ground state in each cluster but also, in principle, all excited states). However, we tried an extrapolation scheme and we computed results to the thermodynamic limit ($l \rightarrow \infty$). Lastly, we define the thermodynamic limit system size corresponding to a specific cluster size ($L \rightarrow \infty$ for a fixed l) as the the smallest system size for which the results do not change if we increase it further. It is rigorously shown[‡] that for the Heisenberg Hamiltonian and clusters of even dimensions, the thermodynamic limit system size of cMF is twice as large as the cluster size in each dimension of the rectangle, and for cPT2 and cCCSD, it is three times larger.

B. cMF results

We start by considering the cMF results. It is important to note that some of these results are already published in Ref. 39. All calculations in this section were performed in periodic square lattices. Only uniform tiling schemes were considered; clusters were rectangles of l lattice sites, each filled with l spins. All the results are assumed to be at the thermodynamic limit $L \rightarrow \infty$ for a fixed l , as explained in the previous section. We note that broken-symmetry cMF solutions can be achieved, that is, a non-zero magnetization develops

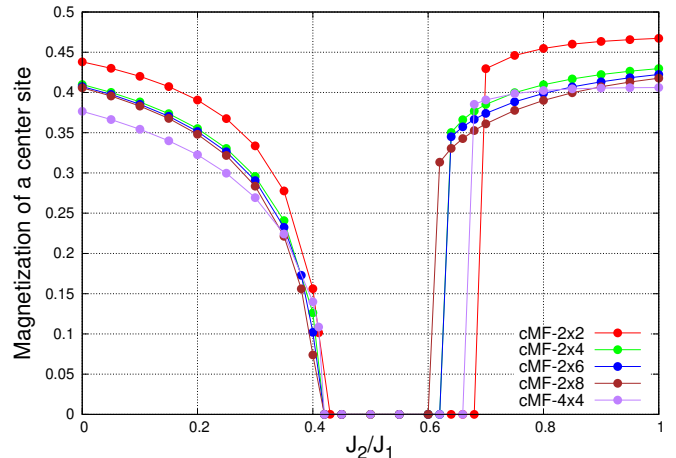


FIG. 3. The magnetizations of a center site for different cluster sizes are shown. The Néel (on the left) and the collinear (on the right) antiferromagnetic phases can easily be observed as there is strong magnetization. In between, there is a non-magnetic phase, which is depicted by the zero magnetization.

on each lattice site. Regarding the collinear case and the rectangular clusters, the collinear correlations are observed in the smaller dimension. This was chosen because its energy was lower than the case with collinear correlations in the larger dimension. We present in Fig. 3 the magnetizations of a center site (for the 2x2 case every site is equivalent) in cMF calculations for different values of l and J_2/J_1 . For readers not familiar with spin systems, magnetizations are equivalent to spin densities. For recognizing the critical points, we compared the paramagnetic and the antiferromagnetic solutions and saw whether their energy difference changes sign. Different cluster sizes correspond to different critical points, so an extrapolation scheme is needed to compute the phase transition points of the thermodynamic limit ($L \rightarrow \infty$ and $l \rightarrow \infty$). This was performed in Ref. 39 and it was shown that cMF was comparable to other methods in the field.

In Figs. 4-6 we demonstrate the energy per site obtained in cMF calculations for different values of l and J_2/J_1 in the thermodynamic limit ($L \rightarrow \infty$). Fig. 4 describes the convergence of $2 \times N$ to the $2 \times \infty$ limit. It is interesting that in this case the second critical point is at ~ 0.6 , while the square lattices (see Fig. 6) seem to predict a slightly greater point. For the square lattices with odd L we notice that there is no sharp transition to a paramagnetic regime. Lastly, Fig. 5 describes the convergence of $4 \times N$ to the $4 \times \infty$ limit. In this case, the values predicted for the second transition point are the largest.

We emphasize the significance of the choice of the cluster, which can be pointed in two different cases. First, the 2x2 cluster results are significantly different from all the other results, which suggests that at the cMF level, 2x2 clusters are not sufficiently large to capture all the physics of the system (luckily this is not the case for the correlated methods, as we shall see later). Second, comparing the 2x8 to the 4x4 clusters, we notice that each phase can be better studied by a different cluster shape, although the total number of sites is the same.

[‡]This is based on the fact that the cMF solution is uniform (same wavefunction on every cluster) for the specific model for clusters of even dimensions. Also, cPT2 and cCCSD only correlate neighbor tiles; there are no Hamiltonian matrix elements between separated tiles. Therefore, it follows that cPT2 and cCCSD yield the thermodynamic limit energy with a 3x3 supracluster lattice.

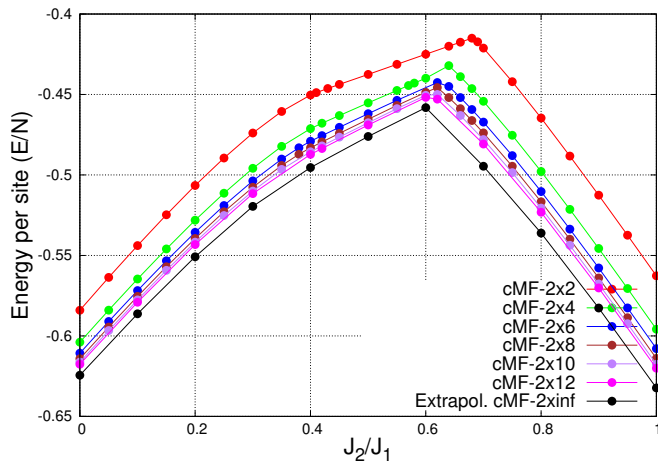


FIG. 4. Energies per site at the cMF level for different cluster schemes are shown, with every cluster having one dimension equal to 2. cMF-2x2 stands for cluster mean-field with 2x2 tiles, etc. The purpose of this figure is to show the convergence of 2xN to the 2x ∞ limit (black circles), extrapolated as described in Sec. III B.

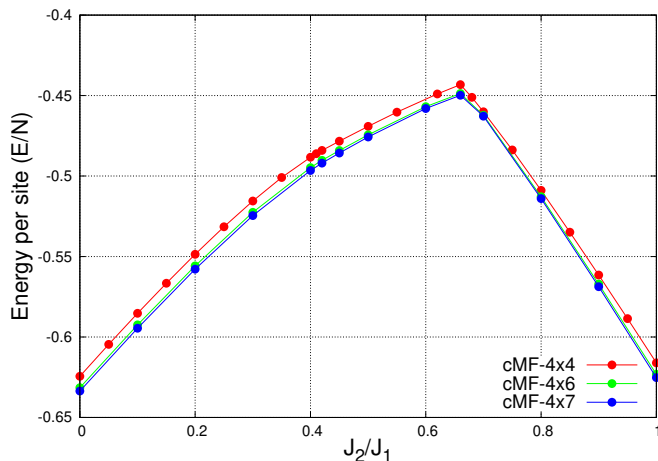


FIG. 5. Energies per site at the cMF level for different cluster schemes are shown, with every cluster having one dimension equal to 4. cMF-4x4 stands for cluster mean-field with 4x4 tiles, etc. The purpose of this figure is to describe the convergence of 4xN to the 4x ∞ limit.

This probably occurs because of the long-range order of the collinear phase, which is better depicted in the 2x8 case. One important observation to point out is that the paramagnetic solution is exactly equivalent to the energy of a single tile with open boundary conditions: ie, in cMF the inter-cluster interaction vanishes as there is no magnetization along the cluster boundaries.

In this work, we also went one step beyond and tried to extrapolate the cMF energy to the thermodynamic limit ($L \rightarrow \infty$ and $l \rightarrow \infty$). In order to achieve that, we plotted the cMF energy with respect to $1/N$ (note that $N = l/x$, where x is one of the dimensions of the cluster). Figures 7 and 8 show a nearly linear behavior as the size of the cluster increases,

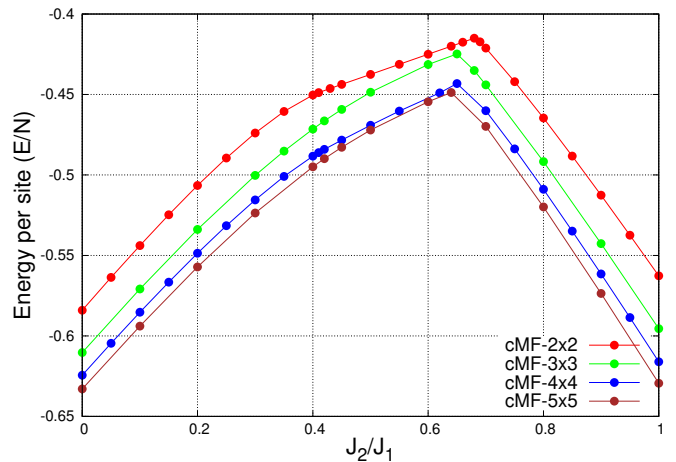


FIG. 6. Energies per site at the cMF level for different square cluster schemes are shown. cMF-2x2 stands for cluster mean-field with 2x2 tiles, etc. The purpose of this figure is to describe the convergence of the NxN to the $\infty \times \infty$ limit.

which can also be explained rigorously*. The $J_2/J_1 = 0$ limit has been well studied with careful extrapolations carried out by several methods (see Ref. 20 and references therein). Our results are summarized in Tab. I. It is shown that they generally agree with other methods in the field (Ref. 25, 32) and the agreement with reference calculations (Ref. 20) is accurate to $(0.001 - 0.002) \times J_1$. Lastly, an extrapolation of the magnetization of the central site was attempted using a $1/N$ behavior and square lattices, similar to the energy. The resulting extrapolated magnetization (for $J_2/J_1 = 0$) in the thermodynamic limit (both $L \rightarrow \infty$ and $l \rightarrow \infty$) is 0.320, which is in good agreement with 0.310 from Ref. 20.

Clusters	cMF (E/N)
2x ∞	-0.62445
3x ∞	-0.63836
4x ∞	-0.64584
5x ∞	-0.65035
6x ∞	-0.65341
$\infty \times \infty$ (1)	-0.66873
$\infty \times \infty$ (2)	-0.66789
Reference Ref. 20	-0.67010
CCM Ref. 25	-0.66936
QMC Ref. 32	-0.66944

*The difference between a 2x6, a 2x8 and a 2x10 tile lies in the addition of extra "internal" sites in the tile, ie., the boundaries have very similar magnetizations. If this is the case, then the error in the energy of the 2xN vs 2x ∞ should behave linearly, as observed in the plot. On the other hand, the linear nature of the NxN extrapolation with respect to $1/N$ can be explained because the error is proportional to the surface (or in this case the perimeter) of the cluster.

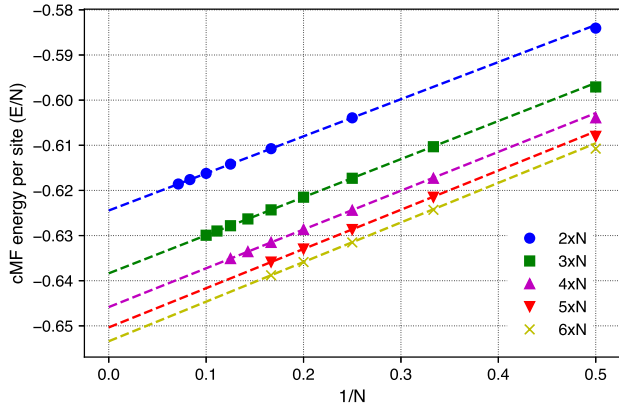


FIG. 7. Energy per site obtained in cMF calculations for $J_2/J_1 = 0$ as a function of the inverse of the cluster size N . It is shown that the behavior is nearly linear, so the extrapolation scheme is reliable. Accurate estimates of the energies for the $2x\infty$, $3x\infty$, $4x\infty$, $5x\infty$ and $6x\infty$ clusters can be computed.

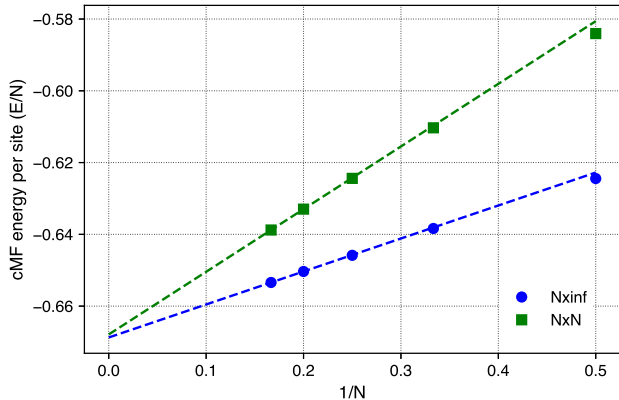


FIG. 8. Energy per site obtained in cMF calculations for $J_2/J_1 = 0$ as a function of the inverse of the cluster size N . $Nx\infty$ energies refer to the extrapolated energies depicted in Fig. 7 and NxN refer to energies computed with square clusters. The extrapolated results at $(1/N = 0)$ were obtained by fitting a line using the two largest cluster sizes in each series and can be compared with extrapolated reference calculations from Ref. 20 (see Tab. I.)

TABLE I. Energy per site obtained by extrapolating cMF calculations at $J_2/J_1 = 0$. $\infty x\infty$ (1) is the result from extrapolating $Nx\infty \rightarrow \infty x\infty$, and $\infty x\infty$ (2) is the result from extrapolating $NxN \rightarrow \infty x\infty$. The extrapolated result from exact diagonalizations (reference calculations) from Ref. 20 is shown for comparison, as well as coupled-cluster (CCM) and quantum Monte Carlo (QMC) results. The agreement with Ref. 20 is accurate to $(0.001 - 0.002) \times J_1$.

C. cPT2 results

We continue by considering the cPT2 results. All the computational parameters are the same as for the cMF results. We remind the reader that all the possible excited states were used to compute the cPT2 energy, except for the $4x4$ case where fewer states[¶] were used. It was ensured, however, that the energy was converged to at least 4 decimals, compared to when using all the states. The criterion for choosing those states was their corresponding eigenvalues, from which we chose the lowest ones. In Fig. 9 we demonstrate the energy per site obtained for different values of l and J_2/J_1 . Even though cPT2 is not variational, there is evidence that the exact energy is lower than the cPT2 energy, because of the results of Ref. 20. There are three important observations. First, increasing the cluster size is not as important for cPT2 as for cMF. This can be useful for real systems, because for cCCSD, we do not have to use large clusters, whose cost can be prohibitive. We have to underline, however, that for our case, cPT2 and cCCSD should converge to the exact answer as the size of the cluster increases. Second, the energy improves very significantly even for the $2x2$ case, which suggests that a large part of the inter-cluster correlations can be treated perturbatively. Third, even though the second-order critical point does not change significantly with the cPT2 correction, the first-order one shifts significantly to $J_2/J_1 \sim 0.62$, compared to ~ 0.64 for most cMF calculations. Lastly, we also tried to extrapolate the cPT2 correlation energy to the thermodynamic limit ($L \rightarrow \infty$ and $l \rightarrow \infty$). We have to remind the reader that it should approach 0, because clusters of infinite size capture all the energy at the cMF level. Similarly to the cMF analysis, the correlation energy was plotted with respect to the inverse of the cluster size, and at $J_2/J_1 = 0$ we found a correlation energy of -0.00185 , which is reasonably close to the expected 0.

D. cCCSD results

We continue by considering the cCCSD results. All the computational parameters are the same as for the cMF and cPT2 results. We remind the reader that all the possible excited states were used to compute the cCCSD energy. In Fig. 10 we demonstrate the energy per site obtained for different values of J_2/J_1 . We have also included, for comparison, the extrapolated results (to the thermodynamic limit $L \rightarrow \infty$ and $l \rightarrow \infty$) calculated from exact calculations computed in Ref. 20. It is important to note that in the intermediate regime, the extrapolated results are not reliable, for reasons mentioned in Ref. 20 and that is why we do not show them. The energy

[¶]1250 states in each relevant S_z sector were used. More specifically, 1250/12870 states for $S_z = 0$, 1250/11440 for $S_z = +1$, 1250/11440 for $S_z = -1$ and 0 states in other sectors, as the matrix elements vanish in that case. As a result, the total number of states used is 3750 out of 65536 states in the Hilbert space.

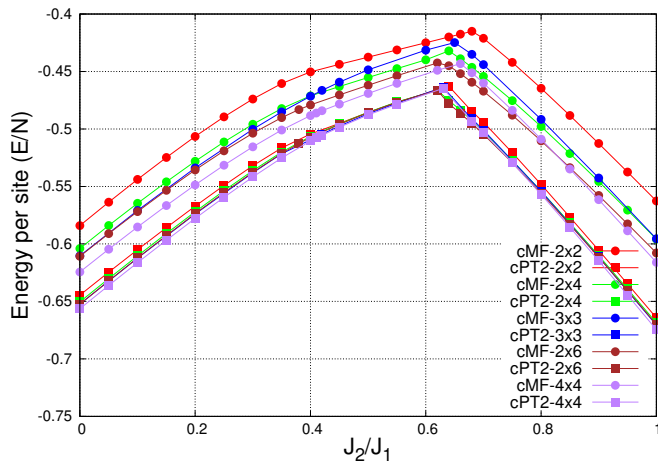


FIG. 9. Comparison of cMF and cPT2 for different cluster schemes is shown. cMF-2x2 stands for cluster mean-field with 2x2 tiles, etc and cPT2-2x2 stands for cPT2 with 2x2 tiles, etc. The circles denote cMF and the squares cPT2. It is worth noting that the cPT2 energies are very close to each other, which suggests that for correlated methods, a minimal cluster size is sufficient.

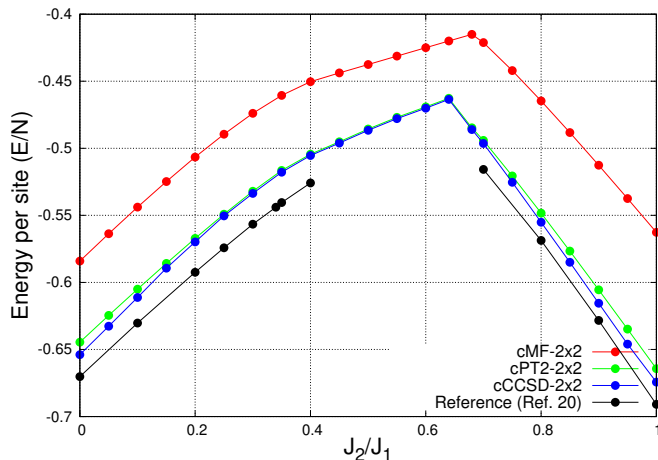


FIG. 10. A comparison between cMF, cPT2 and cCCSD for the energy per site. cCCSD improves the energy significantly compared to cPT2. The exact energy is taken from Ref. 20. Again, we need to emphasize, that in the intermediate regime, the extrapolated results are not reliable (a strange behavior is also depicted in the graph).

improves compared to the cPT2 energy in the two antiferromagnetic phases, but the correction is minimal for the paramagnetic phase. We think that this is due to the nature of the paramagnetic phase (see introduction for the debate of the nature of the paramagnetic phase), which suggests that there exist correlations that cannot be captured by using just 2x2 tiles and a low order coupled-cluster theory. One can argue that the improvement over cPT2 is relatively small considering the error of cPT2. This may imply that triples or quadruples are needed (discussed in the following section). We have to emphasize, however, that at some point cCC should become exact.

V. DISCUSSION

In Sec. II, we have described the cluster mean-field approach to treat strongly-correlated spin systems. A cMF state is used as a variational ansatz for the ground state wavefunction, which is guaranteed by construction to provide better variational estimates than HF when the size of the cluster is larger than 1. Because of the simple cluster language, a RS-PT scheme can be easily adopted to account for the missing inter-cluster correlations. The results presented in Secs. IV B, IV C, and IV D provide evidence that a cluster-based approach can (semi)-quantitatively capture the physics of the ground state of the 2D square $J_1 - J_2$ Heisenberg model. Due to the nature of the Heisenberg Hamiltonian, contributions to the second-order energy arise only from two-cluster spin interactions. From calculations performed in 1D (not in the manuscript), cMF, cPT2 and cCCSD are not as efficient for 2D as for 1D. A significant improvement to the ground state energy is obtained with cPT2 as well as cCCSD, which gives the best results. We also notice that enlarging the size of the cluster in mean-field calculations is worse than performing a cPT2 or a cCCSD calculation. The good quality of cPT2 and cCCSD results suggest that the zero-th order Hamiltonian is suitable for describing spin lattices, at least for the antiferromagnetic regimes.

In the rest of this section we discuss possible strategies that can improve the results presented in this article. The simplest strategy, also discussed in Ref. 8, is to use the full Hilbert space (not restricted to a given S_z sector). This will give significantly more variational freedom to the cMF ansatz. This approach, however, requires a Hilbert space of much larger dimension. As regards the cPT2 and the cCCSD methods, the most straightforward way to go beyond those is to use cPTn or cCCSDTQ, etc. To do so, we must truncate the number of states used, because the computational cost will be prohibitive. This truncation scheme could be either based on the local character of the clusters or can be found stochastically. Another possible route could be to exploit locality. For example, we can treat the interaction between nearest-neighbor clusters with cCC and with further clusters with cPT. One more advantage of the cluster-based approaches, is that even though we have used those approaches to study strongly interacting systems, they may be used in other contexts. More specifically, systems which can be effectively represented in terms of weakly interacting fragments of strongly-correlated subsystems can be very efficiently described by cPT2 or cCCSD. Lastly, another route for correlating cMF would be to write the ansatz as a linear combination of different cMFs of different tilings. This has been tried for dimers by Garcia-Bach⁴² and has yielded very promising results.

VI. CONCLUSIONS

In this work, the optimization of the cluster mean-field state has been carried out with the restriction that the cluster state has well-defined S_z quantum number. The restrictions are imposed in order to preserve total S_z in the full system and fa-

cilitate the computation of the matrix elements. The cluster product state constitutes an eigenstate of a mean-field (zero-th order) Hamiltonian, which allows us to go beyond mean-field in a perturbative and a coupled-cluster framework. We have presented mean-field, second-order perturbative and coupled-cluster results of the ground state energies (and magnetizations) of the square 2D Heisenberg model in the thermodynamic limit ($L \rightarrow \infty$). Also, we have presented a very accurate extrapolation scheme for thermodynamic limit ($L \rightarrow \infty$ and $l \rightarrow \infty$) energies. In general, we observe that cPT2 energies with small clusters are often better than cMF results with significantly larger ones, and the same applies to cCCSD. Overall, the results of this work suggest that a cluster mean-field approach can provide an excellent starting point and a path to a highly accurate, efficient description of strongly-correlated systems, while cPT2 and cCCSD provide an accurate quantitative description. Several strategies to improve the mean-field description as well as correlated approaches built on top of it have been suggested.

ACKNOWLEDGMENTS

This work was supported by the U.S. Department of Energy, Office of Basic Energy Sciences, Computational and Theoretical Chemistry Program under Award No. DE-FG02-09ER16053. CAJH is grateful for support from a start-up package at Wesleyan University. G.E.S. acknowledges support as a Welch Foundation Chair (Grant No. C-0036).

DATA AVAILABILITY

The data that support the findings of this study are available from the corresponding author upon reasonable request.

- ¹S. Sharma, K. Sivalingam, F. Neese, and G. K.-L. Chan, "Low-energy spectrum of iron-sulfur clusters directly from many-particle quantum mechanics," *Nature Chem* **6**, 927–933 (2014).
- ²D. Gatteschi, R. Sessoli, and J. Villain, *Molecular nanomagnets*, Mesoscopic physics and nanotechnology No. 5 (Oxford University Press, 2006).
- ³J. Wu, T. G. Schmalz, and D. J. Klein, "An extended Heisenberg model for conjugated hydrocarbons," *The Journal of Chemical Physics* **117**, 9977–9982 (2002).
- ⁴J. L. Dye, "Electrides: From 1D Heisenberg Chains to 2D Pseudo-Metals," *Inorg. Chem.* **36**, 3816–3826 (1997).
- ⁵A. B. Van Oosten, R. Broer, and W. C. Nieuwpoort, "Heisenberg exchange in La₂CuO₄," *Int. J. Quantum Chem.* **56**, 241–243 (1995).
- ⁶I. W. Bulik, T. M. Henderson, and G. E. Scuseria, "Can Single-Reference Coupled Cluster Theory Describe Static Correlation?" *J. Chem. Theory Comput.* **11**, 3171–3179 (2015).
- ⁷P. W. Anderson, "The Resonating Valence Bond State in La₂CuO₄ and Superconductivity," *Science* **235**, 1196–1198 (1987).
- ⁸C. A. Jiménez-Hoyos and G. E. Scuseria, "Cluster-based mean-field and perturbative description of strongly correlated fermion systems: Application to the one- and two-dimensional Hubbard model," *Phys. Rev. B* **92**, 085101 (2015).
- ⁹L. Isaev, G. Ortiz, and J. Dukelsky, "Hierarchical mean-field approach to the J₁-J₂ heisenberg model on a square lattice," *Phys. Rev. B* **79**, 024409 (2009).
- ¹⁰E. Schrödinger, "Quantisierung als Eigenwertproblem," *Ann. Phys.* **384**, 361–376 (1926).
- ¹¹I. Shavitt and R. J. Bartlett, *Many-body methods in chemistry and physics: MBPT and coupled-cluster theory*, Cambridge molecular science (Cambridge University Press, 2009).
- ¹²S. Li, "Block-correlated coupled cluster theory: The general formulation and its application to the antiferromagnetic Heisenberg model," *The Journal of Chemical Physics* **120**, 5017–5026 (2004).
- ¹³T. Fang, J. Shen, and S. Li, "Block correlated coupled cluster method with a complete-active-space self-consistent-field reference function: The implementation for low-lying excited states," *The Journal of Chemical Physics* **129**, 234106 (2008).
- ¹⁴J. Shen and S. Li, "Block correlated coupled cluster method with the complete active-space self-consistent-field reference function: Applications for low-lying electronic excited states," *The Journal of Chemical Physics* **131**, 174101 (2009).
- ¹⁵V. Abraham and N. J. Mayhall, "Selected Configuration Interaction in a Basis of Cluster State Tensor Products," *J. Chem. Theory Comput.* **16**, 6098–6113 (2020).
- ¹⁶J. I. Cirac and F. Verstraete, "Renormalization and tensor product states in spin chains and lattices," *J. Phys. A: Math. Theor.* **42**, 504004 (2009).
- ¹⁷H. Bethe, "Zur Theorie der Metalle: I. Eigenwerte und Eigenfunktionen der linearen Atomkette," *Z. Physik* **71**, 205–226 (1931).
- ¹⁸E. Dagotto and A. Moreo, "Phase diagram of the frustrated spin-1/2 Heisenberg antiferromagnet in 2 dimensions," *Phys. Rev. Lett.* **63**, 2148–2151 (1989).
- ¹⁹H. J. Schulz and T. A. L. Ziman, "Finite-Size Scaling for the Two-Dimensional Frustrated Quantum Heisenberg Antiferromagnet," *Europhys. Lett.* **18**, 355–360 (1992).
- ²⁰J. Richter and J. Schulenburg, "The spin-1/2 J₁-J₂ Heisenberg antiferromagnet on the square lattice: Exact diagonalization for N=40 spins," *Eur. Phys. J. B* **73**, 117–124 (2010).
- ²¹L. Capriotti and S. Sorella, "Spontaneous Plaquette Dimerization in the J₁ - J₂ Heisenberg Model," *Phys. Rev. Lett.* **84**, 3173–3176 (2000).
- ²²M. Mambrini, A. Läuchli, D. Poilblanc, and F. Mila, "Plaquette valence-bond crystal in the frustrated Heisenberg quantum antiferromagnet on the square lattice," *Phys. Rev. B* **74**, 144422 (2006).
- ²³H. J. Schulz, T. A. Ziman, and D. Poilblanc, "Magnetic Order and Disorder in the Frustrated Quantum Heisenberg Antiferromagnet in Two Dimensions," *J. Phys. I France* **6**, 675–703 (1996).
- ²⁴D. Schmalfuß, R. Darradi, J. Richter, J. Schulenburg, and D. Ihle, "Quantum J₁ - J₂ Antiferromagnet on a Stacked Square Lattice: Influence of the Interlayer Coupling on the Ground-State Magnetic Ordering," *Phys. Rev. Lett.* **97**, 157201 (2006).
- ²⁵R. Darradi, O. Derzhko, R. Zinke, J. Schulenburg, S. E. Krüger, and J. Richter, "Ground state phases of the spin-1/2 J₁ - J₂ Heisenberg antiferromagnet on the square lattice: A high-order coupled cluster treatment," *Phys. Rev. B* **78**, 214415 (2008).
- ²⁶R. F. Bishop, D. J. J. Farnell, and J. B. Parkinson, "Phase transitions in the spin-half J₁ - J₂ model," *Phys. Rev. B* **58**, 6394–6402 (1998).
- ²⁷H.-C. Jiang, H. Yao, and L. Balents, "Spin liquid ground state of the spin-1 2 square J₁ - J₂ Heisenberg model," *Phys. Rev. B* **86**, 024424 (2012).
- ²⁸V. Murg, F. Verstraete, and J. I. Cirac, "Exploring frustrated spin systems using projected entangled pair states," *Phys. Rev. B* **79**, 195119 (2009).
- ²⁹J.-F. Yu and Y.-J. Kao, "Spin-1 2 J₁ - J₂ Heisenberg antiferromagnet on a square lattice: A plaquette renormalized tensor network study," *Phys. Rev. B* **85**, 094407 (2012).
- ³⁰L. Wang, D. Poilblanc, Z.-C. Gu, X.-G. Wen, and F. Verstraete, "Constructing a Gapless Spin-Liquid State for the Spin-1 / 2 J₁ - J₂ Heisenberg Model on a Square Lattice," *Phys. Rev. Lett.* **111**, 037202 (2013).
- ³¹L. Capriotti, F. Becca, A. Parola, and S. Sorella, "Resonating Valence Bond Wave Functions for Strongly Frustrated Spin Systems," *Phys. Rev. Lett.* **87**, 097201 (2001).
- ³²A. W. Sandvik, "Finite-size scaling of the ground-state parameters of the two-dimensional Heisenberg model," *Phys. Rev. B* **56**, 11678–11690 (1997).
- ³³M. P. Gelfand, "Series investigations of magnetically disordered ground states in two-dimensional frustrated quantum antiferromagnets," *Phys. Rev. B* **42**, 8206–8213 (1990).
- ³⁴M. E. Zhitomirsky and K. Ueda, "Valence-bond crystal phase of a frustrated spin-1/2 square-lattice antiferromagnet," *Phys. Rev. B* **54**, 9007–9010 (1996).

- ³⁵K. Takano, Y. Kito, Y. Ōno, and K. Sano, “Nonlinear sigma Model Method for the $J_1 - J_2$ Heisenberg Model: Disordered Ground State with Plaquette Symmetry,” *Phys. Rev. Lett.* **91**, 197202 (2003).
- ³⁶V. Lante and A. Parola, “Ising phase in the $J_1 - J_2$ Heisenberg model,” *Phys. Rev. B* **73**, 094427 (2006).
- ³⁷W.-J. Hu, F. Becca, A. Parola, and S. Sorella, “Direct evidence for a gapless Z_2 spin liquid by frustrating Néel antiferromagnetism,” *Phys. Rev. B* **88**, 060402 (2013).
- ³⁸T. Li, F. Becca, W. Hu, and S. Sorella, “Gapped spin-liquid phase in the $J_1 - J_2$ Heisenberg model by a bosonic resonating valence-bond ansatz,” *Phys. Rev. B* **86**, 075111 (2012).
- ³⁹Y.-Z. Ren, N.-H. Tong, and X.-C. Xie, “Cluster mean-field theory study of $J_1 - J_2$ Heisenberg model on a square lattice,” *J. Phys.: Condens. Matter* **26**, 115601 (2014).
- ⁴⁰E. R. Davidson, “The iterative calculation of a few of the lowest eigenvalues and corresponding eigenvectors of large real-symmetric matrices,” *Journal of Computational Physics* **17**, 87–94 (1975).
- ⁴¹G. E. Scuseria, T. J. Lee, and H. F. Schaefer, “Accelerating the convergence of the coupled-cluster approach,” *Chemical Physics Letters* **130**, 236–239 (1986).
- ⁴²M. Garcia-Bach, “Long-range spin-pairing order and spin defects in quantum spin-ladders,” *Eur. Phys. J. B* **14**, 439–448 (2000).